Self-channeling of high-power laser pulses through strong atmospheric turbulence

J. Peñano, J. P. Palastro, B. Hafizi, M. H. Helle, and G. P. DiComo

Phys. Rev. A **96**, 013829 — Published 14 July 2017

DOI: 10.1103/PhysRevA.96.013829

Self-Channeling of High-Power Laser Pulses Through Strong Atmospheric Turbulence

J. Peñano[1], J.P. Palastro[1], B. Hafizi[1], M.H. Helle[1], G.P. DiComo[2,3]

[1] *Plasma Physics Division, U.S. Naval Research Laboratory, Washington, DC 20375*

[2] *Research Support Instruments, Lanham, MD 20706*

[3] *University of Maryland, College Park, MD 20742*

Abstract

We present a new paradigm for truly long-range propagation of high-power laser pulses through strong atmospheric turbulence. A form of nonlinear self-channeling is achieved when the laser power is close to the self-focusing power of air and the transverse dimensions of the pulse are smaller than the coherence diameter of turbulence. In this mode, nonlinear self-focusing counteracts diffraction, and turbulence-induced spreading is greatly reduced. Furthermore, the laser intensity is below the ionization threshold so that multiphoton absorption and plasma defocusing are avoided. Simulations show that the pulse can propagate many Rayleigh lengths (several kilometers) while maintaining a high intensity. In the presence of aerosols, or other extinction mechanisms that deplete laser energy, the pulse can be chirped to maintain the channeling.

I. INTRODUCTION

Much of our understanding of optical propagation through random media, such as atmospheric turbulence, is based on theoretical and experimental studies where the medium responds linearly to the optical field[1]. The randomness of the medium causes incoherence in the field that, on average, increases the diffractive spreading. As a result, the focusing of light over atmospheric paths with strong turbulence is extremely difficult; even with adaptive optics the beam becomes highly scintillated with a spot size much larger than the diffraction limit[2].

With the advent of laser pulses exceeding gigawatts of peak power, nonlinear self-focusing in air and laser filamentation became possible. Numerous studies have shown that filamentation can produce extended optical and plasma structures in air[3–7]. Filamentation allows the laser pulse to propagate many vacuum Rayleigh lengths at high intensity due to a balancing of nonlinear self-focusing, plasma defocusing or harmonic generation, and nonlinear dispersion. Because of the laser intensity and power required for filamentation, the radius of the optical field of a filament at IR wavelengths (e.g., 800 nm) is typically a few hundred microns, so that the Rayleigh length is short (several meters). Furthermore, the filamentation process is highly dynamic, and unsustainable over very long distances because of ionization losses and/or generation of new frequencies. For instance, IR filaments limited to lengths $\approx$ 200m have been observed[8, 9], and more recent work suggests that mid-IR filaments can persist for up to several hundred meters with reduced ionization losses[10].

Previous studies have investigated the effect of turbulence on filamentation and nonlinear self-focusing[11–20]. The majority of these studies investigated cases where the peak laser power is larger than the self-focusing power of air. Recent experiments have also demonstrated filament formation at kilometer ranges[21]. Here, we present a new paradigm for truly long-range nonlinear atmospheric propagation through strong turbulence without filamentation and plasma formation. We will demonstrate that a form of nonlinear self-channeling, i.e., highly collimated propagation over many Rayleigh lengths, is achieved when the laser power is close to the self-focusing power of air and the transverse dimensions of the pulse are smaller than the coherence diameter of turbulence. Because the coherence diameter and laser spot size are centimeters in scale, and because there are no ionization losses, the channeling can persist for several kilometers through strong turbulence. In some parameter

regimes, we show how the coherence of the nonlinearly channeling beam can be described quantitatively using simple expressions derived for linear propagation, but with an effective Rayleigh length that is dependent on the laser power. Furthermore, with extinction mechanisms that deplete laser energy, we show that a chirped pulse can be used to maintain the channeling. Although our study is focused on propagation in atmospheric turbulence, nonlinear channeling can occur in any optical Kerr medium in which there are random refractive index perturbations.

II. NONLINEAR CHANNELING CONCEPT

The distribution of scale sizes in atmospheric turbulence can be modeled by the Tatarskii spectrum[1] for refractive index fluctuations, i.e., the Fourier transform of the covariance of refractive index fluctuations is $\Phi_n(\kappa) = 0.033 C_n^2 \kappa^{-11/3} \exp(-0.03\kappa^2 \ell_0^2)$, where κ is the wavenumber of the fluctuation, C_n^2 is the structure constant, and ℓ_0 is the inner scale that characterizes the smallest turbulent eddy size. It is assumed that the outer scale is much larger than the beam size and its effects can be neglected. As a wave propagates through turbulence, its optical coherence is degraded. The transverse coherence radius of a plane wave with wavenumber k that propagates a distance L through Kolmogorov turbulence, i.e., where effects of the inner and outer scales can be neglected, is given by $\rho_0 = (1.46 k^2 C_n^2 L)^{-3/5}$. The Rytov variance $\sigma_R^2 = 1.23 C_n^2 k^{7/6} L^{11/6}$ and the dimensionless constant $\Lambda = 2L/(kW^2)$ parameterize the regimes of weak and strong optical fluctuations, with $\sigma_R^2 > 1$ or $\sigma_R^2 \Lambda > 1$ denoting the regime of strong optical fluctuations[22]. W denotes the beam spot size at distance L in the absence of turbulence, and is usually calculated using vacuum Gaussian optics.

In principle, a beam with a diameter smaller than ℓ_0, which typically varies from 1 mm to 1 cm, will undergo wander with very little turbulence-induced spreading[1]. However, maintaining such a small spot size is not possible when the laser power P is much less or much greater than the nonlinear self-focusing power of air $P_{NL} = \lambda^2/(2\pi n_0 n_2)$, where λ is the laser wavelength, and n_0 and n_2 are the linear and nonlinear refractive indices, respectively. For >psec pulses with $\lambda = 1\mu$m, $n_2 = 3 \times 10^{-19}$ cm^2/W, $P_{NL} \approx 5$ GW. A collimated, Gaussian beam with $P << P_{NL}$ will spread due to diffraction with a characteristic scale length Z_R, while for $P >> P_{NL}$, turbulence can seed a filamentation instability[17].

Self-channeling requires an initially collimated pulse with a peak power comparable to P_{NL}.The balancing of diffraction and nonlinear self-focusing, to lowest order, is an unstable equilibrium that limits the distance over which the pulse can propagate without either spreading or collapsing into a filament. In the absence of turbulence, the spot size of an initially collimated Gaussian beam evolves according to[23] $W(z) = W_0[1 + (1 - P/P_{NL})(z/Z_R)^2]^{1/2}$, for $P \leq P_{NL}$, where $Z_R = kW_0^2/2$, and W_0 is the initial Gaussian spot size. This suggests that the effective Rayleigh length is $Z_R/\sqrt{1 - P/P_{NL}}$, and when $P = P_{NL}$, diffraction is cancelled by nonlinear focusing. This expression assumes that the beam profile remains Gaussian. The self-focusing length is more accurately described in Ref. [24]. In reality, the beam profile evolves even when $P = P_{NL}$, but for P slightly less than P_{NL}, the beam can propagate for many Rayleigh lengths and retain a significant fraction of its energy within a radius equal to its original spot size. Additionally, the spot size must be small enough to maintain coherence[19].

There are two parameter regimes to consider. The first regime, characterized by $W_0 < (\ell_0, \rho_0)$, produces long-range channeling in which the beam power contained within a radius W_0 remains relatively constant over distances $> 10Z_R$. In this regime, the smallest phase distortions imprinted by the turbulence are larger than the beam spot size. Hence the beam refractively wanders through the turbulence but is held together by nonlinear focusing. Since the inner scale of atmospheric turbulence can be as small as 1 mm, the Rayleigh length and channeling distance in this regime is small from a practical point of view. For example, for $W_0 = 1$ mm and $\lambda = 1\mu$m, a channeling distance of 15 Z_R, which is typically observed in our simulations, is only 47 m. In the second regime, $\ell_0 < W_0 < \rho_0$, phase perturbations that are small compared with the beam spot size scatter energy out of the beam, resulting in an increase of the RMS spot size. However, the center of the beam remains collimated and a significantly larger fraction of its power propagates within a radius W_0, compared to a low-power beam. Coherence lengths in a typical atmosphere with $C_n^2 = 5 \times 10^{-15}$ m$^{-2/3}$ at several kilometers range are approximately 1-3 cm. Hence, assuming the beam radius is 1 cm, a channeling distance of 15 Z_{R0} corresponds to 4.7 km. When $W_0 >> \rho_0$, the effect of nonlinear focusing is negligible and the beam spreads like a low-power beam.

III. CHANNELING SIMULATIONS

We simulate the propagation of a high-power laser pulse through turbulence using the HELCAP code [23, 25], which solves the paraxial equation for the laser electric field envelope A:

$$\left[2ik\left(\frac{\partial}{\partial z}+\alpha\right)-k\beta_2\frac{\partial^2}{\partial\tau^2}+\nabla_\perp^2\right]A=-2k_0^2\delta nA, \tag{1}$$

where $\delta n = \delta n_T + n_2 I$, z is the axial propagation coordinate, $\tau = t - z/v_g$, v_g is the pulse group velocity, α is the atmospheric extinction coefficient (e.g., due to aerosols and air molecules), $\beta_2 = 0.22$ fsec^2/cm is the group velocity dispersion (GVD) coefficient at $\lambda \approx 1\mu$m, and δn_T is the refractive index due to turbulence, which we model as a series of random phase screens with Tatarskii spectral characteristics. To simulate propagation over approximately 15 Rayleigh lengths with adequate resolution, we solve Eq. (1) on a Cartesian grid with 512x512 transverse points, 400 steps in the propagation coordinate z, with 40 uniformly spaced turbulence phase screens along the beam path. Ensemble-averaged quantities are obtained using 10^3 turbulence realizations. The propagation dynamics for finite duration pulses in extinctive environments are complex as we will show in our time-dependent simulations. For now, to illustrate the basic physics of nonlinear channeling, we retain only the terms in Eq. (1) related to transverse focusing, nonlinearity, and turbulence, i.e., we model a beam with no temporal variation ($\partial/\partial\tau = 0$).

A. Propagation without turbulence

Figure 1 shows the fractional power contained within a radius W_0, of an initially collimated Gaussian beam propagating in the absence of turbulence. By definition, a Gaussian beam initially contains $0.86P$ within a spot size W_0. As the beam propagates, the power within W_0, denoted by P_{W_0}, changes depending on the ratio of P/P_{NL}. $P << P_{NL}$ characterizes linear propagation, in which P_{W_0} decreases over a scale distance Z_R. As P increases and becomes comparable to P_{NL}, the beam retains more of its power within W_0 as it propagates. For $P = 0.945P_{NL}$, P_{W_0} is almost constant over 15 Z_R; although not shown in the figure, $P_{W_0}/P > 0.5$ for up to $30Z_R$. However, increasing the power to 0.95 P_{NL} results in over-focusing that leads to filamentation. At $z = 8Z_R$, the beam has collapsed to a dimen-

sion that is not sufficiently resolved in the simulation and, beacuse plasma effects are not included in these simulations, artificial numerical diffraction occurs. Note the very sensitive nature of the channeling to beam power, where a 1.6% change in P/P_{NL} changes P_{W0} by a factor of 2 after $15Z_R$.

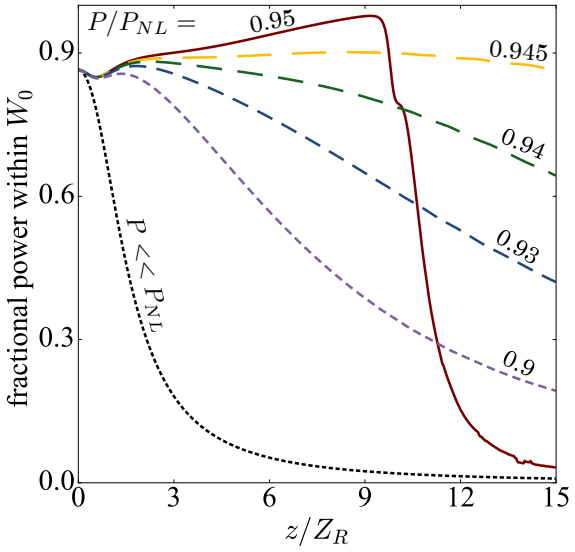

FIG. 1: Simulation results showing fractional power, P_{W_0}/P contained within a radius W_0 (the initial beam radius) as a function of propagation distance z (in units of the Rayleigh length, Z_R) for various powers P (in units of the nonlinear power P_{NL}). The initial beam is collimated and has a Gaussian intensity profile.

B. Propagation in turbulence

We compare the channeling of the beam through turbulence for 3 cases: (1) $W_0/\ell_0 << 1$, (2) $W_0/\ell_0 \simeq 1$, and (3) $W_0/\ell_0 >> 1$, and consider a scaled propagation distance $L = 15Z_R$ with $\sigma_R^2 = 3.0$, and $P = 0.945P_{NL}$.

Figure 2 illustrates the channeling by plotting isosurfaces of normalized beam intensity for a number of representative simulation ensembles. The isosurface plotted is the 0.5 contour of the beam intensity normalized to its peak value at a given z, i.e., the diameter of the surface is the beam's full-width-half-max. The surfaces show that for most cases the beams wander but their radius is relatively constant along the entire path. In a few of the cases shown, the beams either spread, or focus to a filament before propagating the entire path.

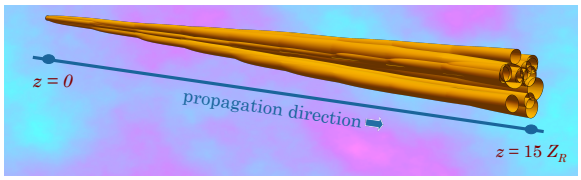

FIG. 2: Simulation results showing isosurfaces of 0.5 times the normalized beam intensity as a function of transverse postion and scaled propagation distance for a representative ensemble of turbulence realizations. The initial beam is collimated with a Gaussian intensity profile and $P = 0.945 P_{NL}$.

Figure 3 plots the channeled power P_{W_0} as a function of propagation distance in the various regimes. In regime (1) turbulence has little effect on the channeling of the beam, i.e., over the entire propagation path, P_{W_0} is almost unchanged relative to its value in the absence of turbulence. As the inner scale is made comparable to (case 2), and then smaller (case 3) than W_0, P_{W_0} decreases. However, even for case 3, the fractional power channeled is much larger than for a low-power beam without nonlinear focusing. Because the turbulence spectrum has an exponential decay near the inner scale, there is little difference between cases (2) and (3). In calculating the ensemble-averaged fractional power that is channelled, we neglect cases where the beam collapses (forms a filament) before propagating the entire range of 15 Z_R. The probability of the beam propagating the entire path without filamenting is approximately 0.86 in case (1), and 0.98 in case (3).

Figure 4 shows the probability distributions of the beam spot size at $z = 15 Z_R$ along with the corresponding ensemble-averaged intensity profiles (with the centroid displacement removed). The standard deviation of the distribution in regime (1) is $\approx 0.5 W_0$, while in regime 2 it is larger at $\approx 2.5 W_0$.

We calculate the coherence radius of the beam, ρ_0, numerically from the degree of coherence (DOC) using Eq.(56) of Ref.[1], i.e., the coherence radius ρ_0 is the transverse distance $|\vec{r} - \vec{r}_c|$ at which the degree of coherence (DOC) function decreases to $1/e$ of its peak value, where $\mathrm{DOC}(\vec{r}_c, \vec{r}, z) = |\Gamma_2(\vec{r}_c, \vec{r}, z)| \left[\Gamma_2(\vec{r}_c, \vec{r}_c, z)\Gamma_2(\vec{r}, \vec{r}, z)\right]^{-1/2}$, $\vec{r}_c$ is the position vector of the beam centroid, $\vec{r}$ is an arbitrary position in the transverse plane of the beam, $\Gamma_2(\vec{r}_1, \vec{r}_2, z) = \langle A(\vec{r}_1, z) A^*(\vec{r}_2, z) \rangle$, and the $\langle\rangle$s denote an ensemble average over many realizations of turbulence. The DOC is defined with respect to the beam centroid with the

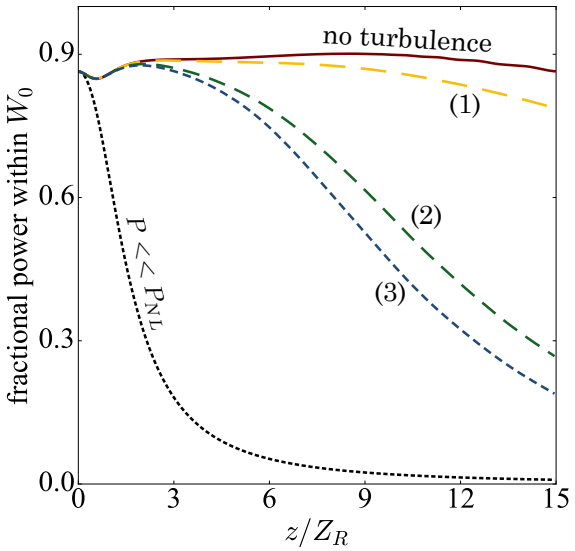

FIG. 3: Ensemble-averaged fractional power, P_{W0}/P, as a function of propagation distance, z (in units of the Rayleigh length, Z_R), for $\sigma_R^2 = 3$, $P = 0.945 P_{NL}$, and (1) $W_0/\ell_0 = 0.1$, (2) $W_0/\ell_0 = 1$, and (3) $W_0/\ell_0 = 10$. Curves representing the case of no turbulence (solid red curve) and diffraction in vacuum (dotted black curve) are shown for comparison.

wander contribution removed. This definition is more appropriate for the describing the physical role of coherence in the channeling process.

Figure 5 plots the coherence radius, the spot size $W = \sqrt{2} W_{RMS}$ (W_{RMS} is the root-mean-squared radius), and full-width-half-max (FWHM) of the beam as a function of scaled propagation distance in the regimes $\ell_0 >> W_0$ (Fig. 5a) and $\ell_0 << W_0$ (Fig. 5b). The coherence radius of the channeling beam in both regimes decreases with propagation distance and is well-described by the coherence radius of a low-power plane wave, which is also plotted for comparison. Note that a collimated, low-power Gaussian beam has a larger coherence radius than a plane wave because as the beam diffracts, the small scale incoherent structures created by turbulence expand. For a channeling beam, however, the beam has near-planar phase fronts, hence its coherence radius is similar to that of a plane wave. Self-focusing becomes less effective as ρ_0 becomes comparable to W. In the case of Fig. 5(a), the coherence radius is larger than W for $L < 10 Z_R$, i.e., the beam remains mostly coherent, and both W and the FWHM are significantly smaller than a diffracting beam. There is a slight increase in the FWHM when the coherence radius becomes smaller than W. The

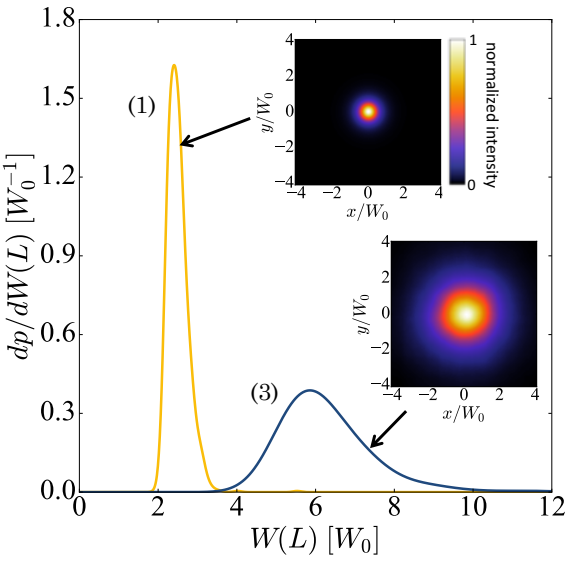

FIG. 4: Ensemble-averaged probability density versus spot size, W (in units of the initial spot size, W_0), after propagating a distance 15 Z_R with $\sigma_R^2 = 3$ and $P = 0.945 P_{NL}$ for cases (1) $W_0/\ell_0 = 0.1$ and (3) $W_0/\ell_0 = 10$ corresponding to Fig. 3. Insets show ensemble-averaged normalized intensity contours for each case. Beam wander has been subtracted to illustrate short-time profiles.

same qualitative behavior is seen in Fig. 5(b) in the regime where $\ell_0 << W_0$, i.e., the FWHM remains relatively constant until the coherence length becomes comparable to W at $L \approx 5Z_R$, at which point the FWHM spreads more rapidly. In both regimes, the beam remains much smaller than the diffraction limit.

In the absence of turbulence, self-channeling of a Gaussian beam produces a non-Gaussian beam profile with a small, central spot, characterized by the FWHM, that is supported by an energy "reservoir" around the beam. In the presence of turbulence, the coherence of this energy reservoir is degraded as the coherence length becomes smaller than the RMS spot size. The central spot holds together while a larger, mostly incoherent "halo" develops, and spreads. As this energy reservoir diffracts away, the central spot starts to spread and channeling is lost. When the inner scale is smaller than the beam radius, the disruption of channeling occurs sooner than when the inner scale is large.

The centroid displacement (wander) of a beam while undergoing nonlinear channeling is shown in Fig.(6) in the parameter regimes $W_0/\ell_0 << 1$ and $W_0/\ell_0 >> 1$. The theoretically predicted wander, $W_c = (2.42 C_n^2 L^3 W_0^{-1/3})^{1/2}$, for a low-power ($P << P_{NL}$), collimated

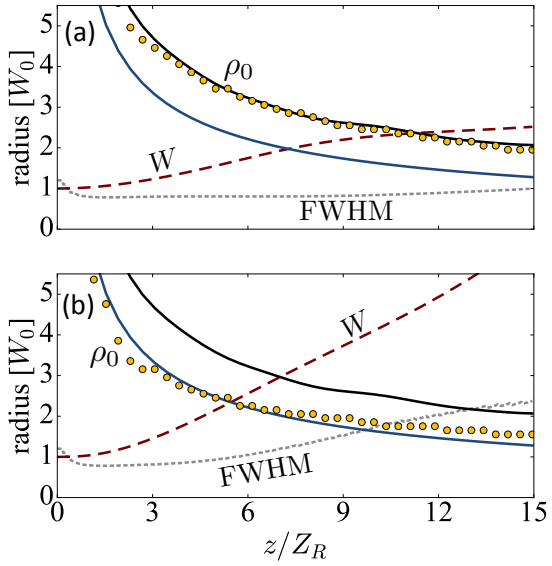

FIG. 5: Ensemble-averaged coherence radius ρ_0 (yellow dots), spot size $W = \sqrt{2}W_{RMS}$ (dashed red curve), and full-width-half-max (FWHM, dotted gray curve) vs. propagation distance, z (in units of the Rayleigh length, $/Z_R$), for $\sigma_R^2 = 3$, and $P = 0.945P_{NL}$, with (a) $W_0/\ell_0 = 0.1$ and (b) $W_0/\ell_0 = 10$. Theoretical low-power plane wave coherence radii for $W_0/\ell_0 = 0.1$ (black curve) and $W_0/\ell_0 = 10$ (blue curve) are also plotted for comparison.

Gaussian beam in the weak turbulence limit, with $W_0/\ell_0 >> 1$, and $\Lambda << 1$, is also shown for comparison. Note that the theoretical curve, which is valid for the regime $\Lambda < 1$ at low-power, adequtely describes the wander of the nonlinearly channeling beam in the regime $\Lambda > 1$ because the collimation provided by nonlinear focusing results in a larger effective Rayliegh length, i.e., small Λ. The same cannot be said of the regime $W_0/\ell_0 << 1$. The ensemble-averaged wander in this regime for low-power propagation is described by $W_c/W_0 = 0.89(L/Z_R)W_0/(\rho_0^{5/6}\ell_0^{1/6})$. If this expression were plotted in Fig.(6), the curve would be very close to the theoretical curve for $W_0/\ell_0 >> 1$. The simulations, however, predict a smaller value of W_c for $W_0/\ell_0 << 1$ compared with linear theory.

IV. CHANNELING WITH ATMOSPHERIC EXTINCTION

So far, we have neglected the temporal dynamics of the pulse. For a pulse in which the peak power $P \approx P_{NL}$, the leading and trailing edges will diffractively spread. Additionally,

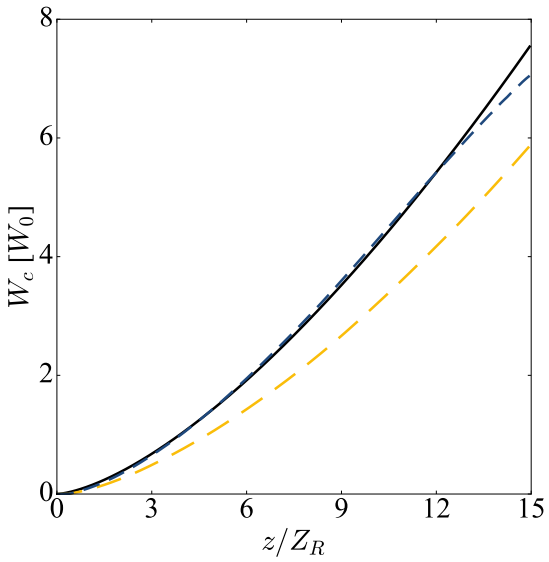

FIG. 6: Ensemble-averaged RMS centroid displacement (wander) versus propagation distance, z (in unit of the Rayleigh length, Z_R), in the regimes $W_0/\ell_0 << 1$ (yellow dashed curve) and $W_0/\ell_0 >> 1$ (blue dashed curve). The solid black curve denotes the theoretical wander of a low-power ($P << P_{NL}$), collimated Gaussian beam in the regime $W_0/\ell_0 >> 1$, $\Lambda << 1$.

in any realistic atmosphere, molecules and aerosols deplete energy from the pulse through absorption and scattering. Given the sensitivity of the self-channeling process to laser power, the pulse must be chirped so that, as energy is lost, it compresses due to the dispersion of air at a rate that preserves the condition $P \approx P_{NL}$. The optimal chirp causes the pulse duration, T, to vary as $\partial T/\partial z = P_{NL}^{-1}(\partial E/\partial z)$, where E is the pulse energy. For a chirp where the frequency varies linearly in time, it is not possible to satisfy this condition along the entire propagation path since the energy decays exponentially with distance, while the pulse duration is, to lowest order, given by[23] $T(z) = T_0\left[(1+\beta_0 z/Z_T)^2 + (z/Z_T)^2\right]^{1/2}$, where $\beta_0 = Z_T/L_T$ characterizes the chirp, $Z_T = T_0^2/(2|\beta_2|)$, L_T is the location of the longitudinal focus, and the initial laser pulse envelope is assumed to have the form $A(0) = A_0 \exp\left[-r^2/W_0^2 - (1+i\beta_0)\tau^2/T_0^2\right]$. For propagation distances $L << \alpha^{-1}$, channeling requires $L_T \approx P_{NL}T_0/(2\alpha E_0)$, where E_0 is the initial pulse energy. In principle, a nonlinear chirp can be used to increase the channeling distance to something comparable to the extinction length.

Even without turbulence, the evolution of the chirped pulse profile is complicated. For

pulses with finite duration, the leading and trailing edges would diffract away, but the region of peak power should be able to channel for many Z_R and be easily observable. An example of this behavior is shown in Fig. 7 which shows the longitudinal and transverse intensity distribution of the laser pulse in the absence of turbulence.

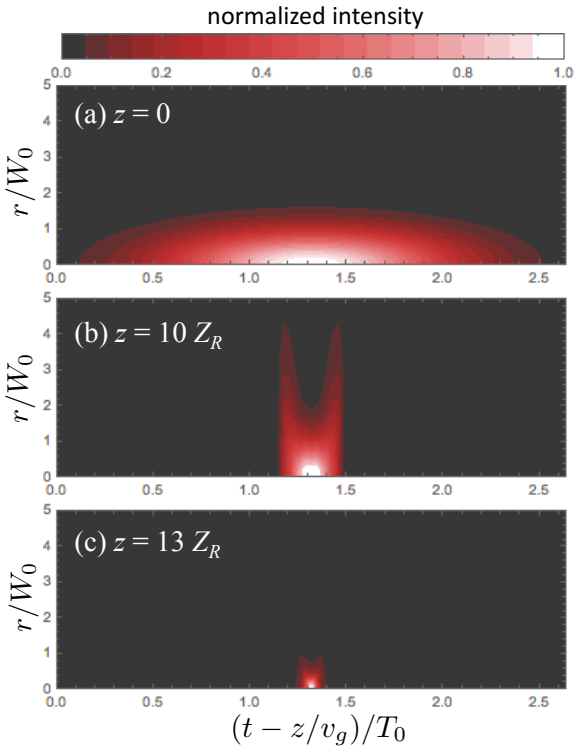

FIG. 7: Simulation result showing laser intensity contours versus radial coordinate, r (in units of the initial spot size, $/W_0$), and axial coordinate, $t - z/v_g$ (in units of initial pulse duration, T_0), for (a) $z = 0$, (b) $z = 10Z_R$, and (c) $z = 13Z_R$. Simulations use a negatively chirped Gaussian pulse with scaled input parameters $L_T/Z_R = 13.2$, $P/P_{NL} = 0.8$, $\alpha Z_R = 0.053$, $n_2 I_0 = 4.8 \times 10^{-10}$, and $Z_R/Z_T = 2 \times 10^{-3}$

In the presence of turbulence, Fig. (8) shows the result of using a negatively chirped Gaussian pulse ($W_0 = 1.4$ cm) with the scaled turbulence parameters $W_0/\ell_0 = 1$ and $\sigma_R^2 = 1.5$. The temporal compression of the pulse keeps the power relatively constant over 6 Z_R. Near the temporal focus at $z = 10Z_R$, the power increases to $5P_{NL}$, but the beam continues to channel with a relatively constant FWHM for at least $12Z_R$. The radius ($\sqrt{2}W_{RMS}$) increases steadily and the fractional power P_{W_0}/P decreases with z but remains well above that of a diffraction-limited beam even though the beam has lost $\approx 55\%$ of its

energy after $12Z_R$. The increasing RMS spot size apparent is due to the rapidly diffracting leading and trailing edges of the pulse, as in Fig. (7).

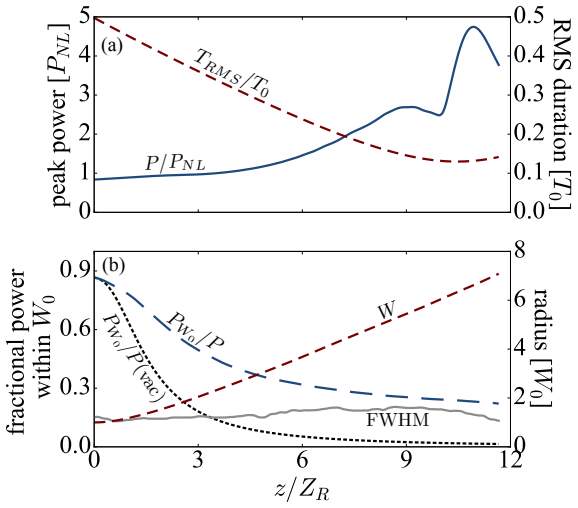

FIG. 8: Panel (a): RMS pulse duration, T_{RMS}, in units of initial pulse duration, T_0, (red dashed curve) and peak power P/P_{NL} (blue curve) vs. propagation distance, z (in units of the Rayleigh length, Z_R). Panel (b) radial FWHM (gray curve), beam radius $W = \sqrt{2}W_{RMS}$ (dashed red curve), fractional power within radius W_0 (dashed blue curve), and fraction power for vacuum propagation (dotted black curve) vs. propagation distance z. Simulations use a negatively chirped Gaussian pulse with the same input parameters as in Fig. 7, and with $\sigma_R^2 = 1.5$, $W_0/\ell_0 = 1$, $\rho_0/W_0 = 1.9$ at $z = 15Z_R$.

V. CONCLUSIONS

In conclusion, we have investigated a new paradigm for transmitting small spot size, high-intensity laser pulses through strong turbulence over many Rayleigh lengths (potentially kilometers). The channeling mechanism relies on 1) using the self-focusing of a collimated pulse with peak power $P \approx P_{NL}$ to overcome diffraction, and 2) a spot size small compared to the coherence length or inner scale of the turbulence to reduce spreading. In the presence of atmospheric extinction, the pulse can be chirped to maintain self-channeling.

Nonlinear channeling can be more effective than using conventional optics to produce a small spot size pulse over long distances in the atmosphere. For example, the long-time-

averaged RMS spot size of a beam focused at a range L in strong turbulence is given by[1] $W_{LT} = W\sqrt{1 + 1.63(\sigma_R^2)^{6/5}\Lambda}$. Consider a situation where the scaled parameters are the same as in Fig. 8. For a low-power beam focused at range $L = 7.2$km, with $W_0 >> \rho_0$, and $\sigma_R^2 = 1.5$, we obtain a highly scintillated beam at range L with $W_{LT} = 0.72(\sigma_R^2)^{3/5}\sqrt{L\lambda} \approx 8$ cm and $FWHM = 13$ cm. Note that for these parameters, a larger W_0 will not result in a smaller focal spot, and that beam wander is a small fraction of W_{LT}. Our results indicate that self-channeling can produce a spot with $W_{RMS} = 5.2$ cm and $FWHM = 1.4$ cm at range, using smaller optics ($W_0 \approx 1.4$ cm) in strong turbulence.

Acknowledgements

The authors acknowledge useful discussions with Drs. A. Schmitt-Sody and J. Elle. J. Penano and M. Helle are supported by the Office of Naval Reserch, J. Palastro and G. DiComo are supported by the High Energy Laser Joint Technology Office, and B. Hafizi is supported by the NRL Base Program.

Appendix

It is useful, for future experimental validation, to examine the sensitivity of the nonlinear channeling mechanism to variations in power and for beam profiles characteristic of a real laser system. Present-day short pulse laser systems are characterized by near-diffraction-limited beam quality ($M^2 \approx 1.2$) and pulse-to-pulse energy stability of $\approx 3\%$. Here, we simulate nonlinear channeling of such a beam.

We measured the transverse intensity profile of a pulse generated by the Astrella laser, a Ti:Sapphire-based ultrashort pulse laser that can output a 1 kHz train of 7 mJ, 40 fsec pulses. The laser intensity profile is well-represented by the sum of two Gaussians, i.e., the initial pulse envelope is modeled as $A(z = 0) = [a_1 \exp(-2r^2/r_1^2) + a_2 \exp(-2r^2/r_2^2)]^{1/2}$. Setting $a_1/a_2 = 1.47$, $r_1/r_2 = 0.7$ results in excellent agreement with the experimental profile of Fig. 9. For comparison, a best-fit Gaussian is also plotted. The residual error resulting from the two-Gaussian fit is five times smaller than for the single Gaussian fit. The experimentally measured M^2 is 1.2. With a perfectly planar phase front, the bi-Gaussian profile has $M^2 = 1.04$. Simulation results using this profile with planar phase fronts are

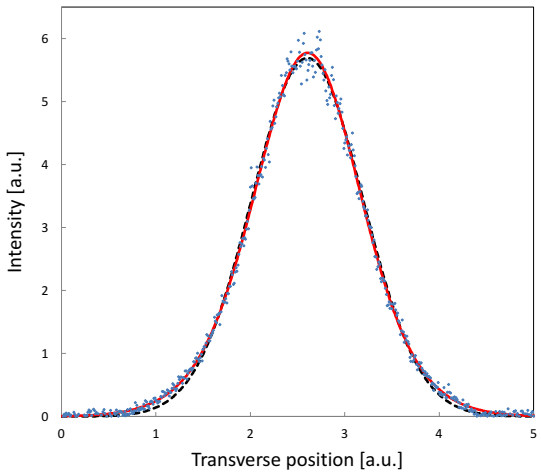

FIG. 9: Measured intensity of laser pulse from Astrella laser (dots) vs. transverse position. A Gaussian best-fit (black curve) and two-Gaussian fit (red curve) are shown for comparison.

markedly similar to those of Fig. 3. To increase M^2 to the experimentally measured value, we imposed a quartic radial variation of the phase. The high-wavenumber noise seen on the experimental profile is an artifact of speckle resulting from the measurement in which the beam is scattered from a rough surface.

We simulated nonlinear channeling of the bi-Gaussian laser profile through turbulence and varied the turbulence inner scale and laser power to observe how channeling is affected. Figure 10 shows the results of plotting the fractional power contained in spot size W_0 versus propagation distance. Results are plotted for various inner scale lengths and for two different laser powers which differ by 3%, corresponding to the experimentally observed energy variance.

Comparing the two red curves in panels 1 and 2, the results show a high sensitivity to beam power in the absence of turbulence. At a power of 1.06 P_{NL}, the fractional power contained in W_0 first decreases as the beam expands, and then increases as nonlinear self-focusing focuses the beam so that the fractional power after propagating 15 Z_R is approximately equal to its initial value. However, for a power that is 3% lower, self-focusing is not as effective and the fractional power in W_0 after 15 Z_R decreases by a factor of 4, i.e., the effective spot size increases by a factor of 2. A qualitatively similar result is seen for turbulence in which the inner scale is large compared to the spot size (yellow curves). Then

the inner scale is comparable to or smaller than the spot size, the sensitivity to power is decreased. For both powers plotted, the effective spot size increases by a factor of 2-3 over 15 Z_R. The beam is still significantly more collimated that the diffraction-limited case in which the spot size increases by a factor of 21.

---

[1] L. C. Andrews and R. L. Phillips, *Laser Beam Propagation through Random Media, Second Edition (SPIE Press Monograph Vol. PM152)* (SPIE Publications, Bellingham, Washington, 2005), 2nd ed., ISBN 0819459488.

[2] J. W. Hardy, *Adaptive Optics for Astronomical Telescopes* (Oxford University Press, New York, NY, 1998), ISBN 9780195090192.

[3] A. Braun, G. Korn, X. Liu, D. Du, J. Squier, and G. Mourou, Optics letters **20**(1), 73 (1995).

[4] A. Couairon and A. Mysyrowicz, Physics Reports **441**, 47 (2007).

[5] S. Eisenmann, E. Louzon, Y. Katzir, T. Palchan, A. Zigler, Y. Sivan, and G. Fibich, Optics express **15**(6), 2779 (2007).

[6] J. Palastro, T. Antonsen Jr, and H. Milchberg, Physical Review A **86**(3), 033834 (2012).

[7] N. Jhajj, E. Rosenthal, R. Birnbaum, J. Wahlstrand, and H. Milchberg, Physical Review X **4**(1), 011027 (2014).

[8] B. La Fontaine, F. Vidal, Z. Jiang, C. Chien, D. Comtois, A. Desparois, T. Johnston, J.-C. Kieffer, H. Pépin, and H. Mercure, Physics of Plasmas **6**(5), 1615 (1999).

[9] G. Méchain, A. Couairon, Y.-B. André, C. D'Amico, M. Franco, B. Prade, S. Tzortzakis, A. Mysyrowicz, and R. Sauerbrey, Applied Physics B **79**(3), 379 (2004).

[10] P. Panagiotopoulos, M. Kolesik, and J. V. Moloney, Physical Review A **94**(3), 033852 (2016).

[11] V. P. Kandidov, O. G. Kosareva, M. P. Tamarov, A. Brodeur, and S. L. Chin, Quantum Electronics **29**, 911 (1999).

[12] S. Chin, A. Talebpour, J. Yang, S. Petit, V. Kandidov, O. Kosareva, and M. Tamarov, Applied Physics B **74**(1), 67 (2002).

[13] R. Ackermann, G. Méjean, J. Kasparian, J. Yu, E. Salmon, and J.-P. Wolf, Opt. Lett. **31**(1), 86 (Jan 2006).

[14] R. Salame, N. Lascoux, E. Salmon, R. Ackermann, J. Kasparian, and J.-P. Wolf, Applied Physics Letters **91**(17), 171106, 171106 (3 pages) (2007).

[15] A. Houard, M. Franco, B. Prade, A. Durécu, L. Lombard, P. Bourdon, O. Vasseur, B. Fleury, C. Robert, V. Michau, *et al.*, Phys. Rev. A **78**, 033804 (Sep 2008).

[16] G. Fibich, S. Eisenmann, B. Ilan, Y. Erlich, M. Fraenkel, Z. Henis, A. Gaeta, and A. Zigler, Opt. Express **13**(15), 5897 (Jul 2005).

[17] J. Penano, B. Hafizi, A. Ting, and M. Helle, J. Opt. Soc. Am. B **31**(5), 963 (May 2014).

[18] D. Eeltink, N. Berti, N. Marchiando, S. Hermelin, J. Gateau, M. Brunetti, J. P. Wolf, and J. Kasparian, Phys. Rev. A **94**, 033806 (Sep 2016).

[19] J. Palastro, J. Penano, W. Nelson, G. DiComo, L. Johnson, M. Helle, and B. Hafizi, Optics Express **24**, 18817 (2016).

[20] B. Hafizi, J. Peñano, J. Palastro, R. Fischer, and G. DiComo, Optics Letters **42**(2), 298 (2017).

[21] M. Durand, A. Houard, B. Prade, A. Mysyrowicz, A. Durécu, B. Moreau, D. Fleury, O. Vasseur, H. Borchert, K. Diener, *et al.*, Optics express **21**(22), 26836 (2013).

[22] L. C. Andrews, R. L. Phillips, and C. Y. Hopen, *Laser Beam Scintillation with Applications (SPIE Press Monograph Vol. PM99)* (SPIE Publications, Bellingham, Washington, 2001), ISBN 0819441031.

[23] P. Sprangle, J. R. Peñano, and B. Hafizi, Phys. Rev. E **66**, 046418 (Oct 2002).

[24] J. Marburger, Progress in Quantum Electronics **4**, 35 (1975).

[25] J. R. Peñano, P. Sprangle, B. Hafizi, A. Ting, D. F. Gordon, and C. A. Kapetanakos, Physics of Plasmas **11**(5), 2865 (2004).

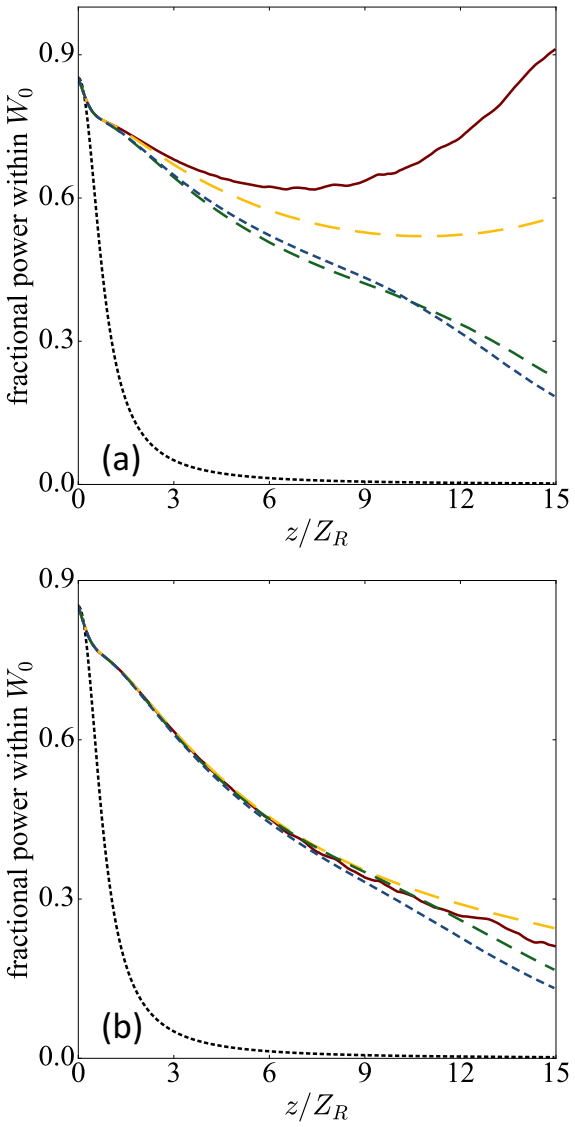

FIG. 10: Ensemble-averaged fractional power contained within the initial beam radius W_0 as a function of propagation distance, z (in units of the Rayleigh length, Z_R), for (a) $P = 1.06P_{NL}$, and (b) $P = 1.03P_{NL}$. The Rytov variance $\sigma_R^2 = 3$ at $z = 15Z_R$. Curves represent $W_0/\ell_0 = 0.1$ (yellow dashes), (2) $W_0/\ell_0 = 1$ (green dashes), and $W_0/\ell_0 = 10$ (shorter dashes). Curves representing the case of no turbulence (solid red curve) and diffraction in vacuum (dotted black curve) are shown for comparison.